J. Fluid Mech. (1980), *vol.* 100, *part* 1, *pp.* 161–184
Printed in Great Britain

On surface pressure fluctuations beneath turbulent flow round bluff bodies

By P. A. DURBIN AND J. C. R. HUNT

Department of Applied Mathematics and Theoretical Physics,
University of Cambridge, Silver Street,
Cambridge CB3 9EW

(Received 2 April 1979 and in revised form 29 August 1979)

Rapid distortion theory is used to calculate surface pressure fluctuations beneath a turbulent flow incident on a two-dimensional bluff body. These pressures depend on the ratio, L_∞/a, of integral scale to body dimension: we give results in the two asymptotic limits $L_\infty/a \gg 1$ and $L_\infty/a \ll 1$. The large-scale limit is described by 'quasi-steady' theory – which we review here; and for the small-scale limit we introduce a 'quasi-homogeneous', or 'slowly-varying', approximation. The theory is compared with field and laboratory measurements and it is found that most measurements lie between the theoretical asymptotes, following the predicted trends.

A number of general conclusions have been obtained for which there are new physical explanations – and which laboratory and field experiments appear to confirm.

(i) The r.m.s. pressure fluctuations, p', caused by upwind turbulence, decrease in strength with distance from the stagnation point when $L_\infty/a \ll 1$; but p' increases with distance from the stagnation point when $L_\infty/a \gg 1$.

(ii) For a given dimension of an obstacle, a, transverse to the flow field, p' increases as the dimension, b, parallel to the flow field increases. At the stagnation point of an elliptical cylinder, when $L_\infty/a \ll 1$,

$$p' = \tfrac{1}{2}\rho u'_\infty U_\infty (1 + b/a)(L_\infty/a)^{\frac{1}{2}}$$

where u'_∞, U_∞ are the upwind r.m.s. turbulent and mean velocities and ρ is the density.

(iii) The fluctuating pressure has a cross-correlation length in the flow direction a factor of a/L_∞ higher when $L_\infty/a \ll 1$ than when $L_\infty/a \gg 1$. In the axial direction the correlation length is again greater (though this time of the same order in L_∞/a) when the incident turbulence is of small scale than when it is of large scale.

1. Introduction

Hunt's (1973) generalization of rapid distortion theory (RDT) has provided an avenue of approach to theoretical investigation of turbulent flow around obstacles. Being based on the linearized, inviscid equations of hydrodynamics, the theory allows one to pose tractable mathematical problems related to turbulent flows. In his (1973) paper Hunt applied the theory to turbulent flow around a circular cylinder, presenting a lengthy analysis of the spectra and covariances of the velocity field near the cylinder in a range of asymptotic limits. In the present investigation an RDT is developed for

0022-1120/80/4546-1110 $02.00

the fluctuating surface pressures on a bluff obstacle in the asymptotic limits of: (i) large-scale turbulence ($L_\infty/a \gg 1$, where L_∞ is the integral scale of the incident turbulence and (a) is a length scale of the obstacle); (ii) small-scale turbulence ($\epsilon \equiv L_\infty/a \ll 1$). Case (i) is dealt with quite readily using a 'quasi-steady' theory (Hunt 1974; Armitt, unpublished), which we review in § 2. Case (ii) is more difficult to treat.

The main purpose of analysing experimentally unrealistic limits is to indicate the trends in the pressure field as the scale of the turbulence and the scale or the shape of an obstacle are changed. (A most useful feature of these rapid-distortion problems is that experimental results at intermediate scales are usually intermediate between theoretical large-scale and small-scale limits.) The quasi-steady, large-scale limit is well known, but only one or two aspects of the small-scale limit have been explored theoretically hitherto. The new aspects explored here are the variation of pressure spectra, the mean square pressure field and the pressure cross-correlation length around two-dimensional cylinders of arbitrary geometry.

In § 3 we introduce a 'slowly varying', or 'quasi-homogeneous', approximation for small-scale turbulence. Near a surface quasi-homogeneity can be used in the horizontal directions only, because variation on the scale, L_∞, of the turbulence is induced in the normal direction by the surface as it blocks the flow; this inhomogeneity is treated explicitly here.

Our analysis of small-scale turbulence is facilitated by the use of velocity-potential, stream-function (Φ, Ψ) co-ordinates. In this co-ordinate system the mean trajectories of fluid particles and the surface of the body are co-ordinate surfaces. These co-ordinates, therefore, simplify the formulation of our equations, which are derived with aid of the formalism of differential geometry. Differential geometry (or tensor analysis) enables us to formulate precisely our equations for arbitrary bluff obstacles; hence, to lend rigour to our asymptotic analysis. Readers unfamiliar with this transparent technique for analysing equations in curvilinear co-ordinates can 'see through' the covariant notation by imagining covariant derivatives (which we denote by ';') to be partial derivatives (which we denote by ',') with respect to a local co-ordinate system. Thus, if '1' denotes the local stream direction, $U^1_{;1}$ is to be understood as 'the derivative of the streamwise velocity in the direction of the stream'. (*Warning*: superscripts on vectors should not be confused with exponents: U^2 is the velocity in the 2 direction. Having been forewarned, this notation should be clear in context.)

In addition to the work of Hunt (1974), a previous application of RDT to surface pressure calculation was made by Graham (1976) who computed the fluctuating drag on a porous plate in turbulent flow. Durbin & Hunt (1979) used the calculations presented herein to estimate fluctuating drag on solid obstacles in turbulent flow.

Experimental studies of surface pressure fluctuations beneath turbulent flow round circular cylinders have been published by Bruun & Davies (1975) and by Batham (1973). These investigators were primarily interested in modelling forces on obstacles in natural flows so they studied an obstacle with a wide wake. Figure 1 illustrates a typical flow around a bluff obstacle with wake. In order to compare the present theory with experiment it is assumed here that the wake contribution to fluctuating pressures on the front of a cylinder in a turbulent stream is statistically independent of the contribution by incident turbulence; and that the existence of a wake does not significantly alter the mean flow near the front of the cylinder. This problem is examined in the recent comparison of turbulent velocity measurements around a circular

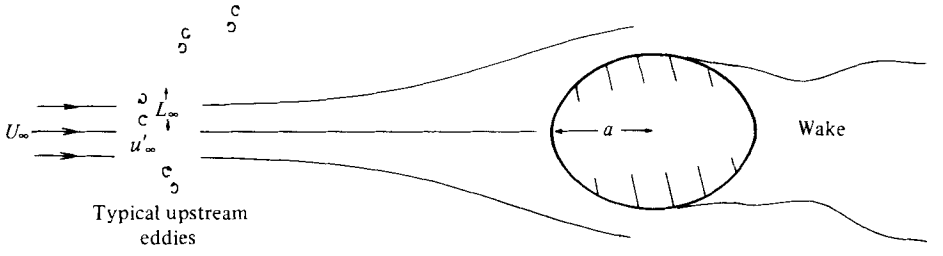

FIGURE 1. Schematic representation of a typical flow around a bluff body.

cylinder with RDT by Britter, Hunt & Mumford (1979). The reader is referred to Hunt (1973) for a comprehensive account of this and other assumptions inherent in RDT: the following lists some additional relevant assumptions.

(i) The upstream turbulence intensity is weak, i.e. $u'_\infty U_\infty \ll 1$.

(ii) Hunt (1973) suggested $u'_\infty/U_\infty \ll L_\infty/a$ as a criterion for linearization of the turbulence distortion. We feel this may be too restrictive, for it is based on a comparison of instantaneous *rates* of vorticity distortion, rather than on *net* distortion. Thus, instead of requiring, as did Hunt, that

$$\left|\frac{(\boldsymbol{\omega}'.\nabla)\,\mathbf{u}'}{(\boldsymbol{\omega}'.\nabla)\,\mathbf{U}}\right| \ll 1$$

we require

$$\left|\frac{\int_{-\infty}^{x}(\boldsymbol{\omega}'.\nabla)\mathbf{u}'\dfrac{dx}{U}}{\int_{-\infty}^{x}(\boldsymbol{\omega}'.\nabla)\,\mathbf{U}\dfrac{dx}{U}}\right| \ll 1. \tag{1}$$

Vortex stretching by the mean flow takes place coherently as vortices approach the obstacle, so the integration in the denominator of (1) can be estimated as $O(a/U_\infty)$. Turbulent vortex stretching occurs coherently only over an Eulerian time scale, T_E, so the integration in the numerator is $O(T_E)$. The Eulerian scale is assumed to be appropriate (in the limit $u'/U \ll 1$) because, ultimately, the turbulence at a *fixed* position is calculated. This scaling leads to the requirement

$$\frac{u'_\infty}{L_\infty} T_E/O(1) \ll 1. \tag{2}$$

Since the Lagrangian time scale, T_L, is $O(u'_\infty/L_\infty)$ (2) becomes

$$T_E/T_L \ll O(1), \tag{3}$$

where, by $O(1)$, we mean an $O(1)$ effect resulting from vorticity distortion by the mean flow. For large eddies $T_E/T_L = O(u'_\infty/U_\infty)$ so condition (ii) reduces to condition (i). For small eddies it is more restrictive. The large eddies, to which the RDT approximations are most applicable, are responsible for pressure fluctuations.

Conditions (i) and (ii) are *suggested* criteria for linearization of the turbulent vorticity equation. For practical purposes, linearization is valid if the turbulence near the

obstacle scales linearly on the turbulence upstream. In flows of present interest this has been observed experimentally to be the case (Bruun & Davies 1975, p. 544).

(iii) The Reynolds numbers $U_\infty L_\infty/\nu$ and $U_\infty a/\nu$ are large.

(iv) The scale of turbulence is large compared with the thickness of the boundary layer on the obstacle.

2. Large-scale incident turbulence: $L_\infty/a \gg 1$

It has been shown by Hunt (1973, 1974) that the leading term in an expansion in a/L_∞, as $a/L_\infty \to 0$, of turbulence properties is described by 'quasi-steady' theory. Quasi-steady theory is based on the assumption that the only effect of turbulence added to the upstream flow will be a small change in angle of incidence and magnitude of the upstream velocity. The perturbation flow is therefore irrotational, with properties directly derivable from potential flow theory. Mean square pressure fluctuations are related simply to mean pressure coefficients and the upstream mean square turbulent velocity fluctuations (Hunt 1974).

The results of quasi-steady theory to be used here are that the mean square pressure fluctuation on a circular cylinder in large-scale (initially isotropic) turbulent flow is

$$\overline{P'^2} = (5 - 4\cos\theta)\, U_\infty^2 \overline{u'^2_\infty} \tag{4}$$

and that the integral scale, L_3^P, along the axial direction is

$$L_3^P = 0{\cdot}5 L_\infty. \tag{5}$$

The formulae (4) and (5) are compared with experimental data in figures 5 and 8.

This quasi-steady theory is particularly simple because the incident vorticity is not distorted by the obstacle, which only 'blocks' the flow, thus producing irrotational velocity fluctuations. When the incident turbulence scale is small, distortion, as well as blocking, becomes important. We now move on to consider this case.

3. Rapid-distortion theory

The RDT as presented by Hunt (1973) hinges on Cauchy's solution of the (linearized) inviscid vorticity equation

$$\tilde{\omega}^{*i}(\mathbf{x}^*, t) = \tilde{\gamma}_j^{*i}\, \tilde{\omega}_\infty^{*j}(\Phi^*, \Psi^*, x_3^*, t^* - \Delta_T^*(\Phi^*, \Psi^*)) \tag{6}$$

with $\tilde{\omega}_\infty^*$ being the vorticity far upstream and

$$(\tilde{\gamma}_j^{*i}) = \begin{pmatrix} \tilde{u}_1^*/u_\infty & -u_\infty\, \partial T^*/\partial x_2^* & 0 \\ \tilde{u}_2^*/u_\infty & u_\infty\, \partial T^*/\partial x_1^* & 0 \\ 0 & 0 & 1 \end{pmatrix}. \tag{7}$$

Equation (6) states, simply, that the vorticity downstream consists of upstream vorticity which has been convected along the mean flow streamlines, $\Psi^* =$ constant. Because vorticity is a vector quantity it has been rotated and stretched in places where the mean streamlines are curved.

In equations (6) and (7) super and subscripts i and j indicate tensor components, the summation convention for repeated subscripts or superscripts being used. The

*'s in (6) and (7) indicate dimensional variables and the tildes will be used for components in $\mathbf{x}^*$ and no tilde for components in Ψ^*, Φ^* co-ordinates. The drift function Δ_T^* was defined by Hunt (1973, and earlier by Lighthill 1956) as the travel time, T^*, of a fluid parcel from upstream infinity to Φ^*, Ψ^* in the presence of the obstacle *less* the travel time over the same range in the absence of the obstacle. Thus,

$$\left.\begin{aligned} T^* &= \lim_{\Phi_0^* \to -\infty} \int_{\Phi_0^*}^{\Phi^*} \frac{d\Phi^*}{|\tilde{U}^*|^2} \\ \text{and} \qquad \Delta_T^* &= \int_{-\infty}^{\Phi^*} \left(\frac{1}{|\tilde{U}^*|^2} - \frac{1}{|U_\infty|^2} \right) d\Phi^*, \end{aligned}\right\} \tag{8}$$

where $|\tilde{U}^*|$ is the magnitude of the mean velocity with respect to x^* co-ordinates. The integrals are to be calculated along a mean-flow stream line.

The fact that Ψ^* and Φ^* appear as arguments in expressions (6) and (8) suggests the efficacy of formulating our theory in Ψ^*, Φ^* co-ordinates. Before doing so it is convenient to introduce non-dimensional variables: U_∞, the uniform mean velocity far upstream of the obstacle, and L_∞, the integral scale of the incident turbulence, will be used to non-dimensionalize velocities and lengths. Let a be a length scale of the obstacle and ϵ denote the ratio L_∞/a. Then the non-dimensional and dimensional variables are related by:

$$\left.\begin{aligned} \mathbf{x}^* = \mathbf{x}L_\infty; \quad \mathbf{k}^* = \mathbf{k}/L_\infty; \quad \tilde{\mathbf{U}}^*(\mathbf{x}^*/a), \tilde{\mathbf{u}}^*(\mathbf{x}^*/L_\infty) = U_\infty(\tilde{\mathbf{U}}(\epsilon\mathbf{x}), \tilde{\mathbf{u}}(\mathbf{x})); \\ t^* = \frac{L_\infty}{U_\infty} t; \quad (T^*, \Delta_T^*)(\mathbf{x}^*/a) = \frac{L_\infty}{\epsilon U_\infty}(T, \Delta_T)(\epsilon\mathbf{x}); \\ (\Psi^*, \Phi^*)(\mathbf{x}^*/a) = \frac{L_\infty U_\infty}{\epsilon}(\Psi, \Phi)(\epsilon\mathbf{x}). \end{aligned}\right\} \tag{9}$$

We now introduce the Ψ, Φ co-ordinate system by defining $X^1 = \Phi/\epsilon$, $X^2 = \Psi/\epsilon$ and $X^3 = x^3$. The functional dependence of $\mathbf{U}$ is of the form $\mathbf{U}(\epsilon\mathbf{X})$, as in (9). So, when $\epsilon \ll 1$, $\mathbf{U}$ is a slowly varying function of $\mathbf{X}$. When measured in this new co-ordinate system the $\tilde{\omega}^i$ of equation (6) become

$$\omega^i = \frac{\partial X^i}{\partial x^j} \tilde{\omega}^j = \frac{\partial X^i}{\partial x^j} \tilde{\gamma}_k^j \tilde{\omega}_\infty^k = \gamma_j^i \omega_\infty^j \tag{10}$$

where $\gamma_j^i = (\partial X^i/\partial x^k)\tilde{\gamma}_j^k$. Thus, in Φ, Ψ co-ordinates,

$$(\gamma_j^i) = \begin{pmatrix} |\tilde{u}|^2 & -|\tilde{u}|^2 \partial T/\partial(\epsilon X^2) & 0 \\ 0 & 1 & 0 \\ 0 & 0 & 1 \end{pmatrix} \tag{11}$$

follows from (7) and the definition of $\mathbf{X}$. The simplicity of (11) as compared with (7) attests to the elegance of working in the $\mathbf{X}$ co-ordinate system. However, this elegance is not achieved without sacrifice; and the sacrifice is that the partial differential equations governing the fluctuating surface pressure field must now be formulated in curvilinear co-ordinates. See appendix A for definitions of the differential geometric notations which will be used in this formulation.

Poisson equation for the pressure

An equation for the pressure can be derived from the inviscid equations of motion for an incompressible, constant-density fluid. In covariant form these equations are

$$-g^{ij}P_{;j} = \frac{\partial}{\partial t}u^i + u^j u^i_{;j}, \tag{12}$$

$$u^i_{;i} = 0 \tag{13}$$

(Lumley 1970). Taking the covariant divergence of (12) using (13) and the identity $g^{ij}_{;k} = 0$ (Hawking & Ellis 1973)

$$\begin{aligned} -g^{ij}P_{;ji} &= u^j_{;i}u^i_{;j} + u^j(u^i_{;ji} - u^i_{;ij}) \\ &= u^j_{;i}u^i_{;j}, \end{aligned} \tag{14}$$

g^{ij} is given in appendix A by (A 1). Linearizing (14) and using the facts that $g^{ij} = 0$, $i \neq j$ and $g^{ii}\Gamma^j_{ii} = 0$:

$$-g^{ii}P_{,ii} = 2U^j_{;i}u^i_{;j}, \tag{15}$$

u and **U** being the turbulent and mean components of the velocity field. Equation (15) is only valid for the present form of metric, for $g^{ii}\Gamma^j_{ii}$ is not in general equal to 0: other terms would, generally, appear on the left-hand side of (15). (This fact that the Laplacian operator retains its form under conformal transformation is well known.) It follows from (9) and (A 4) that

$$\Gamma^i_{jk} = O(\epsilon), \quad U^i_{;j} = O(\epsilon) \quad \text{and} \quad u^i_{,j} = O(1).$$

Thus, to lowest order in ϵ and using the incompressibility ($U^i_{;i} = 0$) and irrotationality ($U^1_{;2} = U^2_{;1}$) of the mean flow,

$$-g^{ii}P_{,ii} = 2\{U^1_{;1}(u^1_{,1} - u^2_{,2}) + U^1_{;2}(u^2_{,1} + u^1_{,2})\}. \tag{16}$$

The terms which have been dropped from (15) involve higher derivatives of **U**, hence (16) has the nature of a 'slowly varying' approximation. Physically, this approximation ignores variations of the turbulent velocity associated with curvature ($u^i_{;j} \sim u^i_{,j}$).

The boundary condition to be used with (16) is obtained from the 2 component of (12) evaluated on $X_2 = 0$ where $u_2 = 0$. Thus, after linearization,

$$-g^{22}P_{;2} = U^1 u^2_{;1} + u^1 U^2_{;1} = 2U^1\Gamma^2_{11}u^1.$$

Thence, by irrotationality and the fact that $P_{;i} = P_{,i}$,

$$-g^{22}P_{,2} = 2u^1 U^1_{;2} \quad \text{on} \quad X_2 = 0. \tag{17}$$

This boundary condition expresses a balance between centrifugal and pressure gradient forces on the curved boundary $X_2 = 0$.

The turbulent vorticity is already known (cf. equation (6)) and the turbulent velocity may be determined from a vector stream function as shown in appendix A. Thus

$$u^i = \eta^{ijk}g_{kk}\psi^k_{;j}, \tag{18a}$$

and to lowest order in ϵ the stream function ψ satisfies

$$-g^{ii}\psi^j_{,ii} = \omega^j. \tag{18b}$$

The boundary condition $u_2 = 0$ on $X_2 = 0$ can be satisfied by appropriately extending the vorticity field inside the surface $X_2 = 0$ (see Batchelor 1967, p. 86). Thus, the right-hand side of the Poisson equation (16) for the pressure can be considered known.

Fourier representation of the turbulence field

Consider the situation depicted in figure 1. The turbulence far upstream of the obstacle may be generated by a grid, downstream of which it becomes very nearly homogeneous and isotropic. Inhomogeneity and anisotropy are the introduced as the turbulence flows around the obstacle. Because the incident turbulence is homogeneous we let the vorticity of the upstream turbulence be represented by the Fourier integral

$$\omega^i_\infty = \iiint_{-\infty}^{\infty} \hat{\omega}^i_\infty(\mathbf{k})\, e^{-i(\mathbf{k}.\mathbf{x}-k_1 t)}\, d^3\mathbf{k}. \tag{19}$$

The inhomogeneous turbulence near the body is represented by

$$\begin{Bmatrix} P \\ u^i \\ \psi^i \end{Bmatrix} = \iiint_{-\infty}^{\infty} \begin{Bmatrix} \hat{P} \\ \hat{u}^i \\ \hat{\psi}^i \end{Bmatrix} (\mathbf{k}, X_2 : \epsilon X_2) \exp\left[-i(k_1 X^1 + k_3 X^3 - k_1(t - \Delta^0_{T/\epsilon}))\right] d^3\mathbf{k} \tag{20a}$$

and

$$\omega^i = \iiint_{\infty-}^{\infty} \hat{\omega}^i(\mathbf{k}, X_2 : \epsilon X_2) \exp\left[-i(k_1 X^1 + k_3 X^3 - k_1(t - \Delta^0_T/\epsilon))\right] d^3\mathbf{k} \tag{20b}$$

where $\Delta^0_T = \Delta_T(X^1, 0)$. (Actually $\Delta^0_T = \infty$ but we may define Δ^0_T as $D^0_T - \lim_{X_2 \to 0} (q \ln X_2)$ where D^0_T is finite.) It follows from (20*b*), (19) and (6) that

$$\hat{\omega}^i = \gamma^i_j \hat{\omega}^j_\infty \exp\left[-i(k_2 X^2 + k_1(\Delta_T - \Delta^0_T)/\epsilon)\right]. \tag{21}$$

Substituting (20) into (16) and equating Fourier coefficients, noting that

$$\partial/\partial X^1(\Delta^0_T + X^1) = 1/|\tilde{u}|^{02} \equiv \Omega^{0-2},$$

(it will not prove necessary to retain an 0 superscript on Ω) gives

$$\hat{P}_{22} - L^2 P = 2\Omega^{-2}(U^1_{;1}(i\Omega^{-2}k_1 \hat{u}^1 + \hat{u}^2_{,2}) + U^1_{;2}(i\Omega^{-2}k_1 \hat{u}^2 - \hat{u}^1_{,2})) \tag{22}$$

to lowest order in ϵ, where $L^2 = \Omega^{-2}k_3^2 + \Omega^{-4}k_1^2$. Similarly, from (18) and (20) we obtain

$$\hat{\psi}^i_{,22} - L^2 \hat{\psi}^i = -\Omega^{-2}\hat{\omega}^i. \tag{23}$$

The boundary condition to (22) is

$$\hat{P}_{,2} = -2\Omega^{-2}\hat{u}^1 U^1_{;2} \tag{24}$$

on $X_2 = 0$. The boundary condition $\hat{u}_2 = 0$ on $X_2 = 0$ and the gauge condition on ψ are satisfied to the present order of approximation by extending $\hat{\omega}^1$ and $\hat{\omega}^3$ antisymmetrically into the boundary and $\hat{\omega}^2$ symmetrically into the boundary. Now, we have shown in (9) that $\mathbf{U}$ is a function of $\epsilon\mathbf{X}$; thus $\Omega(\epsilon\mathbf{X}) \sim \Omega(0) + O(\epsilon)$ and

$$U^1_{;j}(\epsilon\mathbf{X}) = U^1_{;j}(0) + O(\epsilon^2).$$

For this reason the variations of Ω and $U^1_{;j}$ from their surface values may be ignored and (22) may be integrated with the boundary condition (24) treating Ω and $U^1_{;j}$ as

constants. We use a standard Green's function method, putting $X_2 = 0$ in the solution to obtain the pressure fluctuation on the boundary in the form

$$\hat{P}_0 = -2U^1_{;1}\int_0^\infty e^{-\Omega^2 L X_2}(ik_1\Omega^{-2}\hat{u}^1 + L\hat{u}^2)\,dX_2$$

$$+2U^1_{;2}\int_0^\infty e^{-\Omega^2 L X_2}(L\hat{u}^1 - ik_1\Omega^{-2}\hat{u}^2)\,dX_2. \tag{25}$$

A similar solution to (23) for $\hat{\psi}^i$ can be found and then substituted into (25) via (18*a*). To obtain an asymptotic formula for P_0 the expansion of Δ_T about $X_2 = 0$,

$$\Delta_T = -q\ln(\epsilon X^2) + \Sigma(\epsilon X^1) + O(\epsilon X^2 \ln \epsilon X^2) \tag{B 4}$$

derived in appendix B, must be used. (For clarity, we reiterate $\epsilon X^2 \equiv \Psi$, $\epsilon X^1 \equiv \Phi$). The essential feature of (B 4) is the log-singularity. This singularity is characteristic of flows with bluff stagnation points.

A complete analysis of (25) can be found in (Durbin 1979); here we quote the result

$$\hat{P}_0 = \frac{-\Gamma(2+ik_1 q/\epsilon)}{\Omega^4 L^2 m^{(2+ik_1 q/\epsilon)}}\left\{U^1_{;1}\left(ik_1 L\chi_3 - \frac{k_1 k_3}{\Omega^2}\chi_2 - ik_3 L\chi_1 + k_1 L\chi_3\right) + U^1_{;2}\left(\frac{k_1^2}{\Omega^2}\chi_3 - \frac{k_1 k_3}{\Omega^2}\chi_1 + \Omega^2 L^2\chi_3 + ik_3 L\chi_2\right)\right\}, \tag{26}$$

where

$$\left.\begin{aligned} m &= L + ik_2, \\ \chi_1 &= \hat{\omega}^1_\infty \Omega^2 + \left(\frac{\Omega^2 q}{\epsilon} m\hat{\omega}^2_\infty\right)\Big/(1+ik_1 q/\epsilon), \\ \chi_2 &= \hat{\omega}^2_\infty\left(\frac{m}{L(1+ik_1 q/\epsilon)} + 1\right), \\ \chi_3 &= \hat{\omega}^3_\infty. \end{aligned}\right\} \tag{27}$$

One-dimensional spectrum

Having the solution for $\hat{P}_0$ in hand we may now compute spectra and variances of the fluctuating surface pressure field. The one-dimensional spectrum is defined by

$$\Theta_{pp}(k_1) = \iint_{-\infty}^{\infty} \overline{|\hat{P}_0|^2}\,dk_2\,dk_3, \tag{28}$$

where the overbar denotes statistical averaging. This is a frequency spectrum; as usual in RDT, k_1 plays the role of a frequency (i.e. *not* a local wavenumber). The function Θ_{pp} could alternatively have been defined as

$$\frac{1}{2\pi}\int_{-\infty}^{\infty} \overline{P'(t)\,P'(t+\tau)}\,e^{ik_1\tau}\,d\tau.$$

(26) and (27) allow us to evaluate $\overline{|\hat{P}_0|^2}$ once given $\overline{\hat{\omega}^i_\infty \hat{\omega}^j_\infty}$: the pressure field is related statistically to the upstream vorticity. This relation can be represented as

$$\overline{|\hat{P}_0|^2} = \frac{\Omega^{-8}\pi k_1 q/\epsilon(1+k_1^2q^2/\epsilon^2)}{L^4|m|^4\sinh(\pi k_1 q/\epsilon)}\, e^{2k_1 q/\epsilon\xi}\, Q_{ij}\overline{\hat{\omega}^i\hat{\omega}^j}, \tag{29}$$

where the identity $|\Gamma(2+iy)|^2 = (1+y^2)\,\pi y/\sinh(\pi y)$ has been used and $\xi = \tan^{-1}(k_2/L)$. The values of Q_{ij} can be calculated from the expressions

$$\begin{aligned} Q_{ii} &= \alpha_i\alpha_i^* \quad \text{(no summation and * denotes complex conjugation)},\\ Q_{ij} &= (\alpha_i\alpha_j^* + \alpha_i^*\alpha_j), \end{aligned} \tag{30}$$

with

$$\left.\begin{aligned} \alpha_1 &= -U^1_{;2}k_1k_3 + iU^1_{;1}k_3\Omega^2L,\\ \alpha_2 &= U^1_{;1}\Omega^{-2}k_1k_3 + iU^1_{;2}Lk_3 + (1+k_1^2q^2/\epsilon^2)^{-1}\\ &\quad\times\left\{U^1_{;1}\left(\frac{\Omega^{-2}k_1k_3(L+k_1k_2q/\epsilon) - \Omega^2L^2k_3q/\epsilon(Lk_1q/\epsilon - k_2)}{L}\right)\right.\\ &\quad - U^1_{;2}\left(k_1k_3q/\epsilon\left(\frac{L+k_1k_2q}{\epsilon}\right) + k_3(k_2 - Lk_1q/\epsilon)\right)\\ &\quad + iU^1_{;1}\left(\frac{\Omega^{-2}k_1k_3(k_2 - Lk_1q/\epsilon) + \Omega^2L^2k_3q/\epsilon(L+k_1k_2q/\epsilon)}{L}\right)\\ &\quad \left. - U^1_{;2}(-k_3(L+k_1k_2q/\epsilon) + (k_2 - Lk_1q/\epsilon)\,k_1k_3q/\epsilon)\right\}\\ \text{and}\quad \alpha_3 &= U^1_{;2}(\Omega^{-2}k_1^2 + L^2\Omega^2) - iU^1_{;1}2Lk_1. \end{aligned}\right\} \tag{31}$$

These α_i are coefficients of $\hat{\omega}^i_\infty$ in (26) after (27) has been substituted. The form of $\overline{\hat{\omega}^i_\infty\hat{\omega}^j_\infty}(k)$ is restricted by specifying that the upstream turbulence be homogeneous and isotropic:

$$\overline{\hat{\omega}^i_\infty\hat{\omega}^j_\infty} = \frac{3}{8\pi}(|\mathbf{k}|^2\delta_{ij} - k_ik_j)\frac{E(|\mathbf{k}|)}{|\mathbf{k}|^2}. \tag{32}$$

For $E(k)$ we use the von Kármán spectrum

$$\left.\begin{aligned} \tfrac{3}{8}\pi E(\mathbf{k}) &= \beta^2 g_3 k^4/(g_2+k^2)^{17/6},\\ \beta^2 = \frac{\overline{u^2_\infty}}{U^2_\infty};\quad g_2 &= \pi\left(\frac{\Gamma(\frac{5}{6})}{\Gamma(\frac{1}{3})}\right)^2 = 0{\cdot}56;\\ g_3 &= \frac{\Gamma(\frac{17}{6})}{\pi^{\frac{1}{2}}\Gamma(\frac{1}{3})}\,g_2^{\frac{1}{3}} = 0{\cdot}095. \end{aligned}\right\} \tag{33}$$

$\Theta_{pp}(k_1)$ can be computed after equations (29)–(33) are substituted into (28) although the integral must, in general, be evaluated numerically. Low and high wavenumber limits can, however, be determined analytically. (The details of calculation are given in Durbin 1979.)

To lowest order in ϵ†

$$\Theta_{pp}(0) = \left(\frac{U^1_{;1}q}{\epsilon}\right)^2\frac{\beta^2}{(1+\Omega)\,\pi} + O(\epsilon^2). \tag{34}$$

† As a check on our algebra, this result has also been obtained directly from (5.47) of Hunt (1973) (Durbin & Hunt 1979, equations (2.13) and (2.15)).

Note that the right-hand side of (34) is $O(1)$ in ϵ, because $U^1_{;1}$ is $O(\epsilon)$; and that (34) does not depend on the specific form of $E(k)$: it applies to any initially isotropic turbulence. Since $q = (\epsilon/U^1_{;1})_{\text{stagnation}}$ (see appendix B), $\Theta_{pp}(0) = \beta^2/\pi$ at the stagnation point (where, by its definition below (21), $\Omega = 0$).

The low frequency pressures, i.e. the spectrum (34), are produced solely by the $\hat{\omega}^2_\infty$ component of upstream vorticity, and since $k_1 = 0$, by the u_1 component of the upstream velocity. Near the obstacle this vorticity is stretched singularly and rotated into the streamwise direction (Hunt 1973, figure 7), producing large velocity fluctuations normal to the surface. These interact with the mean rate of extension normal to the surface to produce pressure fluctuations (through the term $U^2_{;2}u^2_{;2}$ on the right-hand side of (15)).

As $k_1 q/\epsilon \to \infty$ we find

$$\lim_{k_1 q/\epsilon \to \infty} \Theta_{pp}(k_1) = \frac{2\pi\Gamma(\frac{11}{13})\,\beta^2 g_3}{k_1^{\frac{16}{3}}}\left(\frac{\epsilon}{2q}\right)^{\frac{8}{3}} \Omega^{\frac{10}{3}}((U^1_{;1})^2 + (U^1_{;2})^2). \tag{35}$$

Since $U^1_{;1}$ and $U^1_{;2}$ are $O(\epsilon)\,\Theta_{pp}$ will be $O(\epsilon^{\frac{11}{3}})$ while obeying a $-\frac{16}{3}$ power law in k_1. (This is to be expected since the high frequency spectrum of the surface velocity is proportional to $k_1^{-\frac{10}{3}}$ (Hunt 1973).) In spite of the present derivation this asymptote is valid as $k_1 q/\epsilon \to \infty$ for arbitrary ϵ (as noted by Hunt 1974).

The asymptote (35) is made up of contributions from all three components of the upstream vorticity. This is because the singular straining, which at small k_1 caused $\hat{\omega}^2_\infty$ to predominate, is obscured at large k_1 by the piling up of vortices around the surface of the obstacle (Hunt 1973, figure 7). This complicated mechanism of vorticity distortion leads to a rapid fall-off of Θ_{pp} at high frequency.

At the stagnation point, $\Omega = 0$, (35) does not apply. A detailed analysis of the stagnation point shows that

$$\Theta_{pp} \propto \epsilon^{\frac{2}{3}} k_1^{-\frac{7}{3}}\, e^{-\pi k_1 q/\epsilon} \tag{36}$$

(Hunt 1974; Durbin 1979). (The result of Hunt, 1974, contains an error.) Thus, near the stagnation point piled-up vortices cancel more effectively than at other places around the obstacle and produce an exponentially decaying spectrum. Our analysis of the stagnation point also shows that all the results in this paper, with the exception of (35), are valid there. The facts that our co-ordinate system is singular at $\Omega = 0$ and that the expansion (B 6) is not valid at $\Phi = 0$ are, thus, for the most part irrelevant!

The intensity of pressure fluctuations

The 'slowly varying' approximation for the mean flow yields a consistent approximation to the spectrum at all wavenumbers. Consequently it is not, in general, possible to drop any terms in the rather complex expression (29) for $\overline{|\hat{P}_0|^2}$ or in the integral (28) for Θ_{pp}. However, when variances are being calculated great simplification can be made. The expression

$$\overline{P'^2} = \iiint_{-\infty}^{\infty} \overline{|\hat{P}_0|^2}\, d^3\mathbf{k} \tag{37}$$

contains an exponential dependence on $1/\epsilon$ through the term $\exp\{-k_1 q(\pi - 2\xi)/\epsilon\}$ (equation (29)). Therefore $\overline{P'^2}$ can be obtained accurate to lowest order in ϵ by letting

$k_1 \to 0$ in the integrand in equation (37) keeping $k_1 q/\epsilon = O(1)$. We find that

$$\overline{P'^2} = \frac{\epsilon A^2}{q} I_P + O(\epsilon^3) \tag{38}$$

with

$$I_P = \frac{4}{\pi}\int_0^{\pi}\int_0^{\infty} \frac{\exp\left(-2x\tan^{-1}\left(\frac{\tan\phi}{\Omega}\right)\right)\sin^2\phi\, x\, dx\, d\phi}{(1-e^{-2\pi x})(\sin^2\phi + \Omega^2\cos^2\phi)} \Bigg\} \tag{39}$$
$$= \tfrac{1}{2}$$

where $x = k_1 q/\epsilon$ and $A^2 = [U^1_{;1} q\beta/\epsilon]^2$. This result applies to any initially isotropic turbulence, as did (34). Amazingly, I_P is exactly equal to 0·5 for any Ω. Thus from (38) and (39)

$$\overline{P'^2} = \epsilon A^2/2q. \tag{40}$$

In fact, since $U^1_{;1} q/\epsilon = 1$ at stagnation points, (40) implies a stagnation pressure

$$\overline{P'^2_s} = \beta^2\epsilon/2q. \tag{41}$$

If we use the expression for q derived in appendix C for an elliptic cylinder, assuming that its principle axes are in the ratio $a/b = \gamma$ and that $\alpha = 0$, we find

$$\overline{P'^2_s} = \tfrac{1}{4}\epsilon(\gamma+1)^2\beta^2. \tag{42}$$

When the flow is towards a blunt stagnation point $\gamma \ll 1$ and $P_s^2/\beta^2\epsilon = \frac{1}{4}$; but when the stagnation point is sharp $(P'^2_s/\beta^2\epsilon) \approx \frac{1}{4}\gamma^2 \gg 1$.

The facts that $k_1 q/\epsilon = O(1)$ in (39) and that the spectrum falls off rapidly at high frequency (36) led Durbin & Hunt (1979) to suggest the approximation

$$\overline{P'^2_s} \approx 2\int_0^{\epsilon\pi/4q} \beta^2\Theta^{\infty}_{11}(k_1)\, dk_1 \tag{43}$$

as an interpolation formula valid for all ϵ. This formula reproduces the stagnation-point pressures of (4) and (41) when $\epsilon \to \infty$ and $\epsilon \to 0$ respectively. Using (43) we can generate an approximate form for $\overline{P'^2}$ for arbitrary scales of turbulence (ϵ) and arbitrary obstacle geometry (q, see figure 6).

Cross-stream integral scale

The integral scale, L_3^P, along the body generator is defined by the relation

$$\overline{P'^2} L_3^P = \pi\iint_{-\infty}^{\infty} \overline{|\hat{P}|^2_{k_3=0}}\, dk_1\, dk_2. \tag{44}$$

For the present theory we find

$$\overline{P'^2} L_3^P = \frac{\pi q\beta^2}{3g_2\epsilon}\left((U^1_{;1})^2 + (U^1_{;2})^2\right) + O(\epsilon^2). \tag{45}$$

Equation (45) predicts that $\overline{P'^2} L_3^P$ tends to zero as ϵ tends to zero since the covariant derivatives of U^1 are $O(\epsilon)$. We have seen that $\overline{P'^2}$ is $O(\epsilon)$ as $\epsilon \to 0$ so L_3^P itself is $O(1)$ as $\epsilon \to 0$. Thus, correlations with integral scale comparable to that of the velocity field of the upstream turbulence will be produced when small scale turbulence impinges on a bluff body. It is the $\hat{\omega}^3_{\infty}$ component of vorticity alone which enters the expression

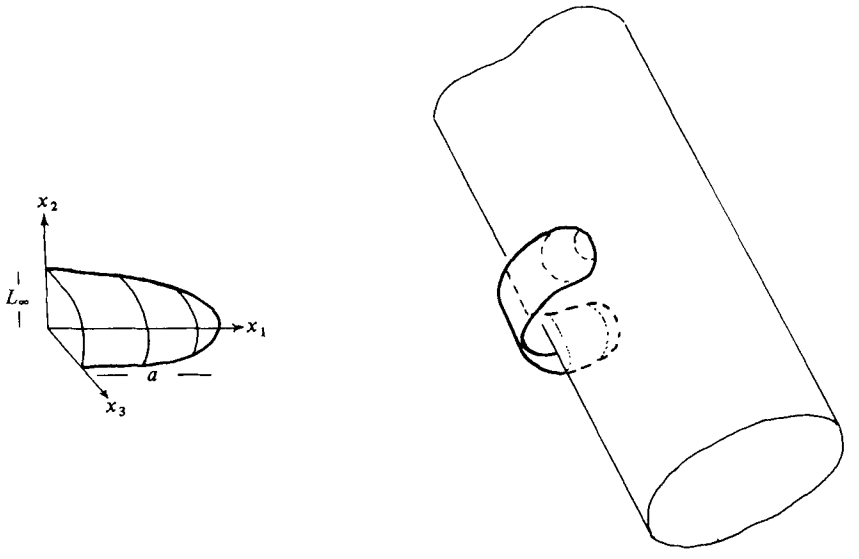

FIGURE 2. The results in (38) and (45) have a straight-forward physical interpretation: owing to distortion, eddies with streamwise length scale, L_∞/k_1, of order (a) make the dominant contribution to $\overline{P'^2}$. But cross-stream dimensions are uneffected by distortion, so their dominant contribution is from $L_\infty/k_3 = O(L_\infty)$. This figure is a schematic representation of the geometry of a 'dominant' upstream eddy far upstream and near to the surface.

(44). Hence, it is the 'piling-up' of upstream vorticity rather than vortex stretching which determines $\overline{P'^2}L_3^P$.

If we define a 'streamwise correlation length', L_1^P, by

$$L_1^P = \pi\Theta_{pp}(0)/\overline{P'^2}$$

we find $L_1^P = O(1/\epsilon)$ (by (34) and (40)); thus correlation lengths in this direction are of the order of the body dimension. It is the $\hat{\omega}_\infty^2$ component of vorticity, being stretched round the cylinder, which is responsible for these long correlations in the streamwise direction.

Figure 2 is a depiction of the geometry of a typical eddy responsible for surface pressure fluctuations. This picture summarizes the physical picture which RDT provides.

4. Discussion and comparison with data

Many experimental measurements have been made around circular cylinders in turbulent flows. Therefore we now reconsider our general formulae in this special case.

When the expressions given in (C 10) are substituted into (34) we obtain the result

$$\Theta_{pp} \sim \frac{\beta^2 \cos^2\theta}{\pi(1+2\,|\sin\theta|)} + O(\epsilon^2), \quad k_1 \to 0. \tag{46}$$

It appears that as one moves away from the stagnation point at $\theta = 0$ the energy in low wavenumbers decreases, becoming $O(\epsilon^2)$ at the top of the cylinder. At high wavenumbers, from (35),

$$\Theta_{pp} \sim \frac{8\pi\Gamma(\frac{11}{3})\,g_3}{k_1^{\frac{16}{3}}}\epsilon^{\frac{11}{3}}|2\sin\theta|^{\frac{10}{3}}\beta^2. \tag{47}$$

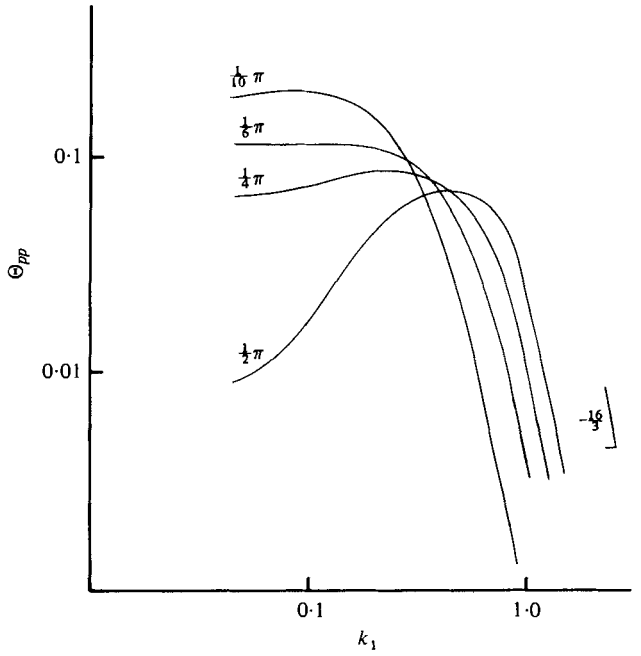

FIGURE 3. Frequency spectra at various angles around a circular cylinder; $\epsilon = 0{\cdot}1$.

Hence we have the opposite trend of Θ_{pp} increasing with θ. The manner in which these two asymptotes connect up has been found by numerical integration of (28). The results are displayed in figure 3.

When $\theta \sim 0$, $\Theta_{pp}(k_1)$ is reasonably flat until $k_1 \sim 0{\cdot}2$. It then drops off rapidly with further increase in k_1. When $\theta \sim \pi/2$, $\Theta_{pp}(k_1)$ has a very very small amplitude when $k_1 < 0{\cdot}1$. It rises away from this low wavenumber level, reaching a peak value when $k_1 \sim 0{\cdot}9$, after which it rapidly transforms into its $-\frac{16}{3}$ high frequency behaviour.

In figure 4 Θ_{pp} has been plotted for various values of ϵ. The curves for $\epsilon = 0{\cdot}05$ and $\epsilon = 0{\cdot}1$ display the ϵ dependence equations (46) and (47) lead one to expect. When $k_1 > 0$, Θ_{pp} increases with ϵ, but the low wavenumber asymptote is independent of ϵ. The curve for $\epsilon = 0{\cdot}4$ might, at first, seem inconsistent with (46). This is not so, for it was obtained by integrating the whole of (29) and hence contains $O(\epsilon^2)$ and higher-order terms. Of course, other $O(\epsilon^2)$ terms have been neglected by the slowly-varying approximation so retaining $O(\epsilon^2)$ terms in figure 4 does not, in principle, improve the accuracy of Θ_{pp}; it still has an error of $O(\epsilon^2)$ at small k_1. The present theory can be used when $\epsilon = 0{\cdot}4$, or larger, but one must remember that it neglects order ϵ^2 terms when doing so.

Recent experiments by Kawai, Junji & Hatsuo (1979) show quite dramatically the reduction of the amplitude of the surface pressure spectrum at frequencies greater than zero as ϵ decreases. Their measurements were at the stagnation point, of two-dimensional square prism, and, as expected, their low frequency asymptotes were independent of ϵ. The slope of Kawai *et al.*'s spectra at high frequency was ≈ -3, somewhat smaller than our $-\frac{16}{3}$ prediction. It is very likely that, at high frequency, nonlinear transfer significantly alters our linear predictions.

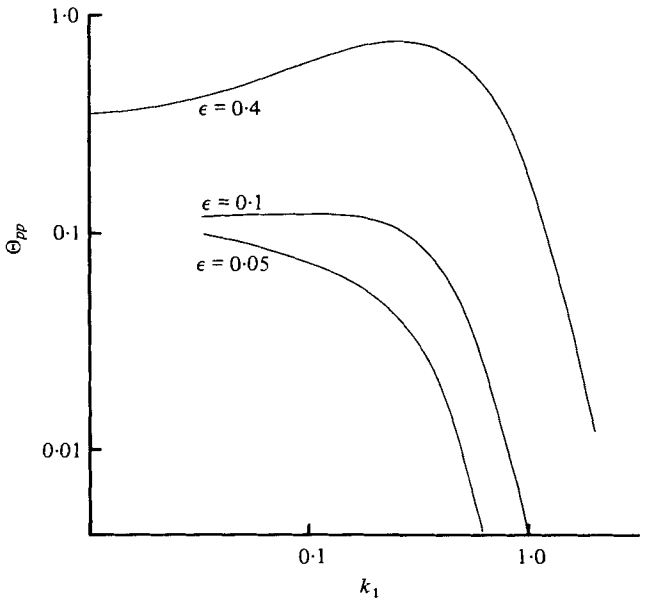

FIGURE 4. The spectrum at $\theta = \frac{1}{8}\pi$ as a function of ϵ.

The formula (40) for $\overline{P'^2}$ shows that

$$p' \equiv (\overline{P'^2})^{\frac{1}{2}} = \epsilon^{\frac{1}{2}}\beta\cos\theta \tag{48}$$

for a circular cylinder. At the front of the cylinder ($\theta = 0$) $p' = \epsilon^{\frac{1}{2}}\beta$ while at the top ($\theta = \frac{1}{2}\pi$) $p' = O(\epsilon^{\frac{3}{2}})$ because $U^1_{;1}$ vanishes there.

In figure 5 $\lim_{\epsilon\to 0} p'(\theta)/\beta\epsilon^{\frac{1}{2}}$ has been plotted along with data from Batham (1973) and Brunn & Davies (1975). In the experiments $u'_\infty/U_\infty = 0{\cdot}1$ and values of ϵ were 1·1, 1·0 and 0·38; as indicated in the figure caption.

The data we have included are from flows which the investigators felt to be critical. (The Reynolds numbers were all greater than 2×10^5, while critical Reynolds numbers were all less than 10^5.) Consequently, these experimental results are independent of Reynolds number, the separation point, and hence the wake, is as far to the rear as possible, and coherent vortex shedding, which might otherwise dominate the measurements, is largely suppressed. These consequences are confirmed by Brunn & Davies' (1975) experiments and by Batham's (1973) experiment using a smooth cylinder. Batham's rough cylinder produced Reynolds number dependent vortex shedding; but his data on p' for $\theta \lesssim 0{\cdot}4\pi$ were independent of Reynolds number, so we have included them in figure 5.

The experimental measurements of p' all show a peak beginning at $\theta \sim \frac{1}{2}\pi - \frac{1}{3}\pi$ and centring on $\theta \sim 0{\cdot}6\pi$. This is associated with unsteadiness of the separation point. Hence, our theory can only be compared with measurements made on the front face of cylinder, $\theta \lesssim \frac{1}{3}\pi$.

The experimental data presented in figure 5 have been adjusted in an attempt to removed pressure fluctuations associated with the wake. On the basis of an assumed

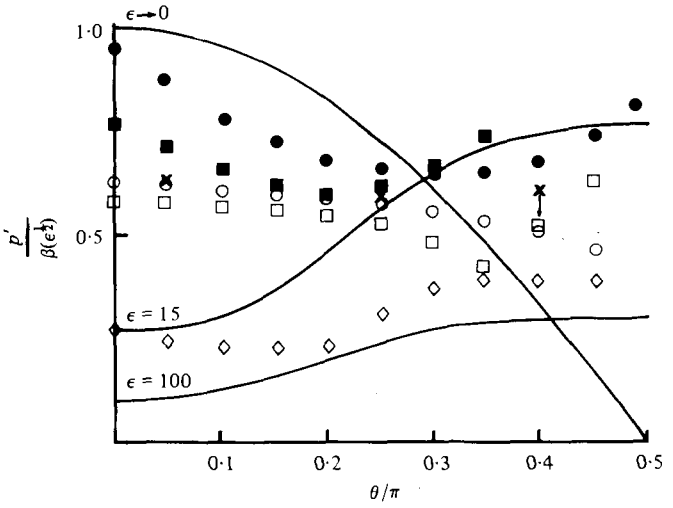

FIGURE 5. Theoretical and experimental r.m.s. pressures: values of ϵ are labelled on the theoretical curves and $\beta \approx 0{\cdot}1$ for all sets of experimental data. The $\epsilon = 0$ curve is our new small-scale result and the curves labelled $\epsilon = 15$ and $\epsilon = 100$ follow from quasi-steady theory. ——, theory; ●, $\epsilon = 0{\cdot}38$; ■, $\epsilon = 1{\cdot}1$ (Bruun & Davies 1975); □, $\epsilon = 1{\cdot}0$ smooth cylinder; ○, $\epsilon = 1{\cdot}0$ rough cylinder (Batham 1973); ◇, $\epsilon = 15$ (Tunstall 1974). The points labelled × are unadjusted values (see (49)) of p' for Batham's rough cylinder.

lack of correlation between contributions by the wake and incident turbulence to p' the adjusted value has been defined as

$$p' = (\overline{P_t'^2} - \overline{P_0'^2})^{\frac{1}{2}}, \tag{49}$$

where P_t' is the pressure measured in a turbulent stream and P_0' that measured in a uniform stream. The difference between p' and $(P_t'^2)^{\frac{1}{2}}$ was invariably small, indicating that pressure fluctuations on the front of the cylinder are largely due to the incident turbulence.

In practice, the wake fluctuations may not be totally uncorrelated with the incident turbulence. This question, in the context of equation (49), has been dealt with comprehensively by Britter *et al.* (1979). In light of their conclusions, and the smallness of our adjustment, we feel (49) to be reasonable. In figure 5 some unadjusted data points – marked by crosses have been included to be compared with the open circles and to illustrate the magnitude of our adjustment.

Tunstall (1974) has shown quite definitely that when $a/L_\infty \ll 1$ the variation of p' with θ is given by quasi-steady theory in which measured values of the mean pressure coefficient, $C_p(\theta)$, are used. His measurements on the chimney at Fawley generating station are shown in figure 5 and compared with the formula (equation (4))

$$p'/\epsilon^{\frac{1}{2}}\beta = (5 - 4\cos^2\theta)^{\frac{1}{2}}/\epsilon^{\frac{1}{2}}, \tag{50}$$

evaluated at $\epsilon = 15$. This formula is based on a potential flow without a wake. When Tunstall used his measurements of C_p – instead of potential flow – to predict p' he found almost perfect agreement with observed values. An evaluation of (50) with $\epsilon = 100$ is also shown in figure 5.

The theoretical curves in figure 5 bracket the laboratory data and at small θ the theoretical trend for $p'/\beta\epsilon^{\frac{1}{2}}$ to decrease with increasing ϵ is reflected in all the data. When θ is near $\frac{1}{2}\pi$ the reverse trend is predicted: $p'/\beta\epsilon^{\frac{1}{2}}$ should increase with ϵ at small ϵ (at large ϵ it decreases as $1/\epsilon^{\frac{1}{2}}$). Because of unsteadiness of the separation point, mentioned earlier, the data in figure 5 cannot be used to verify this trend. The observed angular dependences of p' in figure 5 are certainly similar to those predicted, realizing of course, that the theory applies to extreme values of ϵ.

The extrapolation formula (43) has been evaluated with $q = \frac{1}{2}$ (circular cylinder) and with $q = 2$ (flat plate). It is compared with experimental data in figure 6. In addition to measurements on circular cylinders, included in this figure are measurements on other bluff bodies such as: a two-dimensional flat plate with a filled-in wake (Bearman 1972); a model cooling tower (Propper 1977); the side of a two-dimensional square prism (Lee 1975); and a circular disk (Marshall 1965). The data included in figure 6 broadly follows the tendency of p' to decrease as ϵ decreases. With the exception of the solid triangle, the data points for circular cylinders lie on the appropriate curve ($q = \frac{1}{2}$). Bearman's data for a flat plate also lie on the appropriate curve ($q = 2$). One would expect the open square to lie very nearly on the curve for $q = 2$: it lies just below it. The open diamond was measured in a three-dimensional flow and so cannot be predicted from the present theory. We have not yet been able to obtain theoretical results for three-dimensional obstacles; but this datum point suggests pressure fluctuations would be larger: naturally, one is hard pressed to make such a statement on the basis of one point.

In figure 7 the p' curve for a circular cylinder ($a = b$) has been replotted along with p' curves for elliptical cylinders (with $a = 4b$) with zero and $\frac{1}{2}\pi$ angles of incidence. The curve with $a = 4b$, $\alpha = 0$ is similar to that with $a = b$ although it is flatter for large θ and more peaked at small θ. This is a consequence of the changed angular dependence of $U^1_{;1}$. When $a = 4b$ and $\alpha = \frac{1}{2}\pi$, p' first increases with decrease of θ because $U^1_{;1}$ increases. Near the side of the cylinder ($\theta = 0$) $U^1_{;1} \to 0$; hence p' must also tend to zero. This latter behaviour has been sketched qualitatively with a dashed line in figure 7.

The quantity $\overline{p'^2}L_3^P$ is independent of θ for

$$\overline{p'^2}L_3^P = 2\pi\epsilon\beta^2/3g_2 \tag{51}$$

by (45). (On elliptical cylinders this quantity will have an angular dependence.) The length L_3^P is itself a function of θ and can be calculated from (48) and (51):

$$L_3^P = 2\pi/(1{\cdot}68\cos^2\theta), \tag{52}$$

as is shown by the upper curve in figure 8. The formula (52) depends on the assumed form, (33), of $E(k)$. Therefore, the shape of the curve in figure 8 is more important than its actual magnitude.

The quasi-steady theory gives $L_3^P = 0{\cdot}5$ for large ϵ and isotropic upstream turbulence. This is also shown in figure 8.

Data from Batham (1973) and from Bruun & Davies (1975) have been plotted in figure 8. Only Batham's smooth cylinder data are included since his rough cylinder data (for L_3^P) was dominated by vortex shedding. No adjustments for the wake have been made to the data. Bruun & Davies (1975) found L_3^P to be 'closely related to the

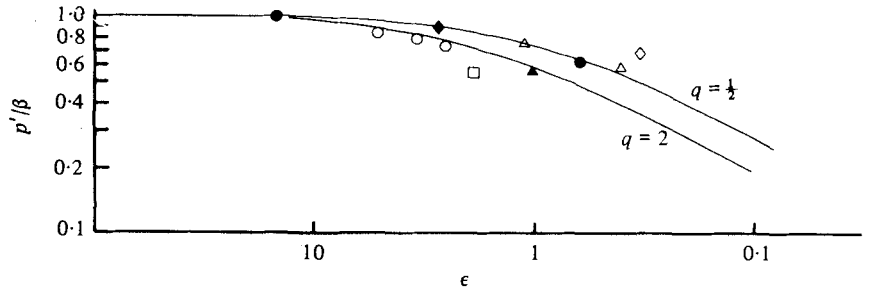

FIGURE 6. R.m.s. stagnation pressures as a function of ϵ. Solid curve, theoretical extrapolation formula (43); ▲, Batham (1973); ○, Bearman (1972); △, Bruun & Davies (1975); □, Lee (1975); ◇, Marshall (1965); ◆, Propper (1977); ●, Tunstall (1974).

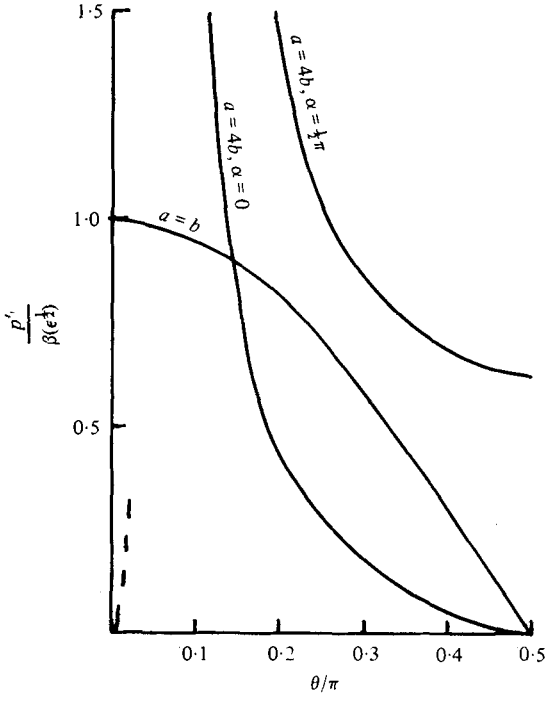

FIGURE 7. Distribution of r.m.s. pressure around elliptical cylinders.

correlation length of the turbulence in the approaching air'; so we suspect such adjustments would be small. We are not certain why there is a lack of agreement between the data of Batham and the data of Bruun & Davies for $\epsilon \approx 1$.

We conclude from figure 8 that again the theory encloses the data, predicts the trend that L_3^P decreases with increasing ϵ, and is suggestive of the observed angular dependence (excluding data points at $\frac{1}{2}\pi$, which are in the separation-dominated region).

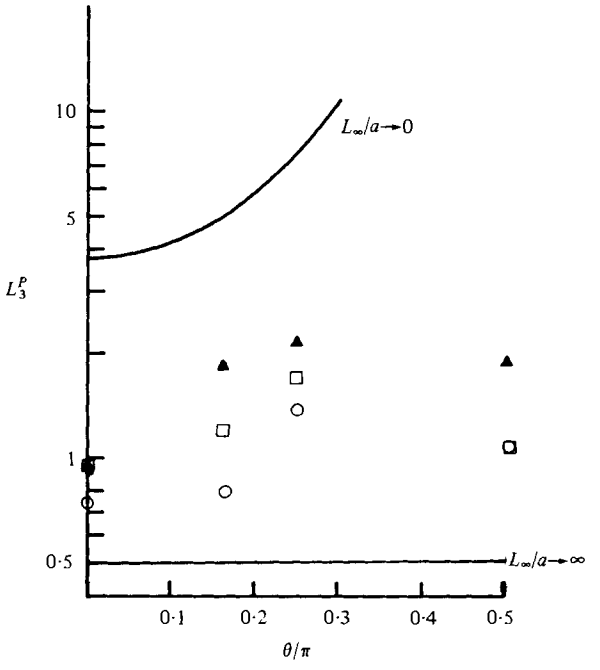

FIGURE 8. Cross-stream integral scales. ——, theory; ▲, $\epsilon = 0{\cdot}38$; ○, $\epsilon = 1{\cdot}1$ (Brunn & Davies 1975); □, $\epsilon = 1{\cdot}0$ (smooth cylinder) (Batham 1973).

Pressure fluctuations p' for cylinder with wake

In § 1 we mentioned our assumption that, for present purposes, alterations of the potential flow near the front of a circular cylinder due to the wake can be ignored. To check our assumption p' has been calculated using Parkinson & Jandali's (1970) potential-flow model for a cylinder with wake.

For the potential flow given by Parkinson & Jandali

$$\left.\begin{aligned} U^1_{;1} &= \frac{\epsilon(2\cos\alpha\cos\theta' + \cos^2\alpha + 1)}{\cos\alpha\,(\cos\delta + \cos\theta')^2} \\ &\quad \times \left\{\frac{2\cos\delta\cos\alpha\,(\cos\theta'\cos\delta + 2\cos\theta' - 1) + (\cos^2\alpha + 1)\,(1 + \cos\theta'\cos\delta)}{(2 + 2\cos 2\theta' + 8\cos\alpha\cos\theta' + 4\cos^2\alpha)^{\frac{1}{2}}}\right\} \\ \text{and} \quad q &= \frac{2(1+\cos\delta)\cos\alpha}{(1+\cos\alpha)\,(1 + 2\cos\delta\cos\alpha + \cos^2\alpha)} \end{aligned}\right\} \tag{53}$$

where

$$\cos\delta = \cos\alpha + \frac{\sin^3\alpha}{k}.$$

α and k are empirical parameters related to separation angle and base pressure coefficient by $\alpha_{\text{sepn}} = \pi - 2\alpha$, $C_{pb} = 1 - k^2$. The variable θ' is a parametric co-ordinate defined by conformal transformation. It is related to the actual angle around the cylinder by

$$\sin\theta = \left[\frac{\sec\alpha + \cos\theta'}{\frac{1}{2}(\sec\alpha + \cos\alpha) + \cos\theta'}\right]\cos\alpha\sin\theta'. \tag{54}$$

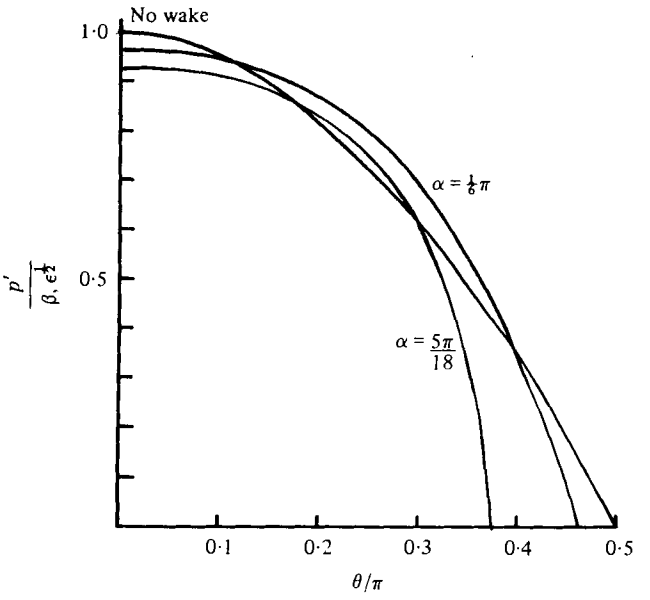

FIGURE 9. Comparison of p' in flows with and without a wake. The curve with $\alpha = \frac{1}{6}\pi$ corresponds to a critical-Reynolds-number wake, $\alpha = 5\pi/18$ to a subcritical wake, and the unlabelled curve to a wakeless flow.

For a wake at critical Reynolds number Parkinson & Jandali used $\alpha = \frac{1}{6}\pi$ and $k = 1{\cdot}175$. (Very nearly these values can be derived from Bruun and Davies' data.) The corresponding profile of p' is compared, in figure 9, with that for a wakeless flow. Also included in figure 9 is the sub-critical case $\alpha = 5\pi/18$, $k = 1{\cdot}4$. At $\theta = 0$ the order of the curves from top to bottom is: no wake, critical wake, and sub-critical wake. The difference between the wakeless flow and the critical flow is small; the discrepancy between theory and data in figure 5 is due more to the finiteness of ϵ and to unsteadiness of the separation point in the experiments than to alterations of the mean potential flow by the wake. Since the stagnation-point formula (43) depends only on q, it might be worth noting that (53) gives $q = 0{\cdot}533$ (little different from $q = \frac{1}{2}$) for a critical wake.

5. Conclusions

New RDT calculations have been presented for surface pressure fluctuations produced by small scale turbulence. The behaviour of small-scale turbulence undergoing distortion was found to differ drastically from that of large-scale turbulence. It can be concluded that predictions of quasi-steady theory are unrealistic when the incident turbulence scale is not large. Indeed, we have found experimental data at intermediate values of ϵ to lie largely between theoretical predictions for $\epsilon \to 0$ and for $\epsilon \to \infty$ (figures 5 and 8). The changes with ϵ in magnitude and angular dependence of experimental values for p' and L_3^P are much as predicted.

Unfortunately, it is not practical to do RDT calculations for intermediate values of ϵ. However, our understanding of turbulence distortion, based on asymptotic solutions, has enabled us to propose a very reasonable extrapolation formula for stagnation-point pressure fluctuations. Figure 6 shows that this formula does a good

job of correlating experimental data. Further interpolation formulae have not yet been found; but our asymptotic solutions are a significant step towards an understanding of distorted turbulence, which we hope will lead to practical prediction techniques.

Appendix A. Relevant differential geometry

A rudimentary discussion of differential geometry with application to the Navier–Stokes equations can be found in an appendix to Lumley (1970) and a more complete discussion also with reference to the equations of hydrodynamics is contained in Hawking & Ellis (1973). The notations used here are taken primarily from the latter reference. Thus, covariant and contravariant vectors are denoted by subscripts and superscripts respectively, e.g. dx_i and dx^i. In obtaining equation (10) we have used that fact that the vorticity vector (which can be written $\omega^i = |\boldsymbol{\omega}|/|d\mathbf{l}|\, dl^i$, cf. Lamb 1932) transforms contravariantly.

A tensor of fundamental importance is the metric, which provides a definition of the length in the **X** co-ordinate system. The components of this tensor are

$$g^{ij} = \frac{\partial X^i}{\partial x_k}\frac{\partial X^j}{\partial x_k}, \tag{A 1}$$

since in our case **x** is a Euclidean co-ordinate system (E^3). The metric also performs the valuable function of interconverting covariant and contravariant vectors: thus $dx^i = g^{ij}\, dx_j$. With the present definitions of **X**,

$$(g^{ij}) = \begin{pmatrix} \Omega^2 & 0 & 0 \\ 0 & \Omega^2 & 0 \\ 0 & 0 & 1 \end{pmatrix}, \tag{A 2}$$

where $\Omega^2 = |\tilde{\mathbf{U}}|^2$. Singular points of the conformal mapping, which are defined as points where $\Omega = 0$, must be excluded from the manifold covered by **X**. Indeed, the analysis in appendix B is not strictly valid within a neighbourhood of $O(\epsilon)$ of stagnation points. To avoid confusion it should be noted that the co-ordinate velocities $\dot{X}^i$ of the mean fluid motion are zero with the exception of $U^1 = \dot{X}^1 = \dot{\Phi}/\epsilon = |\tilde{\mathbf{U}}|^2$. (Recall that the velocity vector in the **x** co-ordinate system is distinguished by a tilde.)

Covariant differentiation will be denoted by ';' and partial differentiation by ','. Thus,

$$U^i_{;j} = U^i_{,j} + \Gamma^i_{jk}\, U^k. \tag{A 3}$$

The Christoffel symbol, Γ^i_{jk}, for the present metric is equal to 0 if i or j or k equals 3 and

$$\Gamma^i_{jk} = -\Omega^{-1}\left(\delta^i_j\frac{\partial\Omega}{\partial X^k} + \delta^i_k\frac{\partial\Omega}{\partial X^j} - \delta^i_k\frac{\partial\Omega}{\partial X^i}\right) \tag{A 4}$$

if $i, j, k \neq 3$. Here δ^i_j is the Kronecker delta.

A skew symmetric tensor, termed the canonical 3-form, can be defined with components

$$\eta_{ijk} = |\mathbf{g}|^{\frac{1}{2}}\epsilon_{ijk}. \tag{A 5}$$

Here $|\mathbf{g}| = \det(g_{ij}) = \Omega^{-4}$. The familiar Euclidean skew symmetric tensor ϵ_{ijk} is equal to

$$6\delta^1_{[i}\delta^2_j\delta^3_{k]} = \delta^1_i\delta^2_j\delta^3_k + \delta^1_j\delta^2_k\delta^3_j + \delta^1_k\delta^2_i\delta^3_j - \delta^i_j\delta^2_i\delta^3_k - \delta^1_k\delta^2_j\delta^3_i - \delta^1_i\delta^2_k\delta^3_j$$

where $[\ldots]$ denotes the components of a skew symmetric tensor. With the present metric

$$\eta^{ijk} = 6|\mathbf{g}|^{-\frac{1}{2}}\delta^{[i}_1\delta^j_2\delta^{k]}_3 \tag{A 6}$$

so

$$\eta^{ijk}\eta_{lmn} = 6\,\delta^i_{[l}\delta^j_m\delta^k_{n]}. \tag{A 7}$$

The vorticity vector, in covariant form, is

$$\omega^i = \eta^{ijk}U_{k;j} \tag{A 8}$$

and if we define the stream function, $\boldsymbol{\Psi}$, by

$$U_k = \eta_{klm}g^{ln}\psi^m_{;n}. \tag{A 9}$$

it follows from (A 7), (A 8) and (A 9) that

$$\begin{aligned}\omega^i &= -\eta^{kji}\eta_{klm}g^{ln}\psi^m_{;nj}\\ &= 6\,\delta^k_{[k}\delta^j_l\delta^i_{m]}g^{ln}\psi^m_{;nj}.\end{aligned} \tag{A 10}$$

For a diagonal metric (A 10) becomes

$$\begin{aligned}\omega^i &= -g^{kk}\psi^i_{;kk} + g^{ik}\psi^j_{;kj}\\ &= -g^{kk}\psi^i_{;kk}\end{aligned} \tag{A 11}$$

if $\boldsymbol{\Psi}$ satisfies the gauge condition

$$\psi^i_{;i} = 0$$

(see Batchelor 1967).

Appendix B. Expansion of the drift function for a bluff body

Our small ϵ expansion requires at one stage the first term of an expansion of the drift function about $\Psi = 0$ when $\Phi \neq 0$. This term need only be determined up to an additive function of Φ.

Consider a bluff body (without circulation). Denoting the complex velocity potential by W it follows from the fact that the half angle at the leading edge of a bluff body is $\frac{1}{2}\pi$ that

$$\frac{dW}{dz} = (-W)^{\frac{1}{2}}f(W) + h(W) \tag{B 1}$$

where f and h are analytic, $f(0) = O(1)$ and $h(W) = O(W)$ as $W \to 0$. Thus we write

$$|\tilde{\mathbf{U}}|^2 \sim |W|/g_0; \quad g_0 = |f(0)|^{-2} \tag{B 2}$$

near the stagnation point, $W = 0$. The drift function is approximated as $\Psi \to 0$ by

$$\Delta_T \sim \int_{-\Phi}^{\Phi} \frac{g_0\,d\Phi}{(\Psi^2+\Phi^2)^{\frac{1}{2}}} + \int_{-\infty}^{-\Phi}\left(\frac{1}{|\tilde{\mathbf{U}}^2(0,\Phi)|} - 1\right)d\Phi - 2\Phi. \tag{B 3}$$

Carrying out the integrations we find

$$\Delta_T \sim -q \ln|\Psi| + O(\Psi \ln \Psi) + \Sigma(\Phi). \tag{B 4}$$

$q = 2g_0$ and $\Sigma(\Phi)$ is an undetermined function of Φ; whose exact form is irrelevant. In writing (B 4) it has been assumed that $\Phi = O(1)$. Thus, the analysis done in this appendix does not apply at the stagnation point; although, as mentioned in the text, most of our results remain valid there.

By definition (see B 2)

$$q = 2g_0 = \frac{1}{|\tilde{\mathbf{U}}| \dfrac{d|\tilde{\mathbf{U}}|}{d|W|}\Big|_{0,0}} = \epsilon / U^1_{;1}|_{\text{stagnation}}; \tag{B 5}$$

alternatively,

$$q = 2|W| \Big/ \left|\frac{dW}{dz}\right|^2_{0,0}. \tag{B 6}$$

If we write W as a function of the complex variable z, defined such that as $z \to z_s$ W and $dW/dz \to 0$ then

$$q = 1/|d^2W/dz^2|_{z=z_s}. \tag{B 7}$$

Appendix C. Evaluation of geometrical terms and velocity derivatives for Elliptical Cylinders

In this appendix we obtain expressions for the mean flow quantities arising in the present theory for the case of flow round an elliptical cylinder. The complex velocity potential, $W(z)$, for the flow round an elliptical cylinder, with principle axes a and b, consisting of a uniform velocity at angle of incidence α far from the surface, is described parametrically by the equations

$$z = \zeta + \lambda^2/\zeta; \quad \lambda^2 = \frac{a-b}{2}, \tag{C 1}$$

$$W = (\zeta e^{-i\alpha} + e^{i\alpha}/\zeta) \tag{C 2}$$

(Batchelor 1967, p. 428). The normalisation used in this appendix is $(a+b)/2 = 1$ and $|\mathbf{U}_\infty| = 1$. In (C 1) z is the co-ordinate system of the ellipse and ζ the co-ordinate system of a circle: the conformal transformation (C 1) defines a one-to-one relation between the co-ordinates of the circle and points of the ellipse. Thus, on the surface of either $\zeta = \exp\{i(\pi - \theta)\}$. The first and second derivatives of W on the surface of the ellipse are

$$\frac{dW}{dz} = \frac{dW}{d\zeta}\frac{d\zeta}{dz} = \frac{2i \sin(\alpha - \theta)}{b\cos\theta - ia\sin\theta}, \tag{C 3}$$

$$\frac{d^2W}{dz^2} = \frac{d^2W}{dz\,d\zeta}\frac{d\zeta}{dz} = \frac{-2\,e^{i\theta}\{e^{-i\alpha}(b\cos\theta - ia\sin\theta) - 2i\lambda^2 \sin(\alpha-\theta)\}}{(b\cos\theta - ia\sin\theta)^3}. \tag{C 4}$$

There are three quantities entering the present theory which are dependent on the geometry of the obstacle. First, we require the covariant derivatives $U^1_{;1}$ and $U^1_{;2}$ on the surface. From (A 3) and (A 4) we find

$$\left.\begin{aligned} U^1_{;1} &= \frac{U^1}{\Omega}\frac{\partial\Omega}{\partial\Phi/\epsilon} = \frac{\epsilon\tilde{\mathbf{U}}.\tilde{\nabla}|\tilde{\mathbf{U}}|}{|\tilde{\mathbf{U}}|} \\ \text{and similarly} \quad U^1_{;2} &= \frac{\epsilon\tilde{\mathbf{U}} \wedge \tilde{\nabla}|\tilde{\mathbf{U}}|}{|\tilde{\mathbf{U}}|}. \end{aligned}\right\} \tag{C 5}$$

Equation (C 5) can be put into a more convenient form by substituting

$$|\tilde{\mathbf{U}}|^2 = (U^1)^2 + (U^2)^2$$

and invoking incompressibility and irrotationality to show that

$$U^1_{;1} + iU^1_{;2} = \epsilon\left(\frac{\tilde{U}^1 - i\tilde{U}^2}{|\tilde{\mathbf{U}}|}\right)^2\left(\frac{\partial\tilde{U}^1}{\partial x^1} + i\frac{\partial\tilde{U}^1}{\partial x^2}\right) = \epsilon\left(\frac{dW/dz}{|dW/dz|}\right)^2\frac{\overline{d^2W}}{dz^2}. \tag{C 6}$$

The overbar in (C 6) denotes complex conjugation. Secondly, we need the geometrical parameter

$$q = \left|\frac{d^2W}{dz^2}\right|^{-1}_{\theta=\alpha} \tag{C 7}$$

(see (B 7)). And, finally, the surface speed

$$\Omega = |\tilde{\mathbf{U}}| = |dW/dz| \tag{C 8}$$

is needed. Substituting (C 3), (C 4) into (C 6) to (C 8) gives

$$U^1_{;1} + iU^1_{;2} = \frac{2\epsilon\{e^{i\alpha-\theta}(a^2\sin^2\theta + b^2\cos^2\theta) - 2i\lambda^2\sin(\theta-\alpha)(1-\lambda^2 e^{-2i\theta})\}}{(a^2\sin^2\theta + b^2\cos^2\theta)^2}, \tag{C 9}$$

$$q = \tfrac{1}{2}(a^2\sin^2\alpha + b^2\cos^2\alpha)$$

and

$$\Omega = \frac{2|\sin(\alpha-\theta)|}{(a^2\sin^2\theta + b^2\cos^2\theta)^{\frac{1}{2}}}$$

where $\epsilon = 2L_\infty/(a^* + b^*)$ and $b = 2 - a$ (* denotes a dimensional variable).

For the special case of a circular cylinder $a = b = 1$, $\alpha = 0$ and

$$\left.\begin{aligned} &U^1_{;1} + U^1_{;2} = 2\epsilon(\cos\theta - i\sin\theta), \\ &q = \tfrac{1}{2}, \\ &\Omega = 2|\sin\theta|. \end{aligned}\right\} \tag{C 10}$$

REFERENCES

Batchelor, G. K. 1967 *An Introduction to Fluid Dynamics*. Cambridge University Press.

Batham, J. P. 1973 *J. Fluid Mech.* **57**, 209.

Bearman, P. W. 1972 *J. Fluid Mech.* **53**, 451.

Britter, R. E., Hunt, J. C. R. & Mumford, J. C. 1979 *J. Fluid Mech.* **92**, 269.

Bruun, H. H. 1973 Univ. Southampton, *Inst. Sound Vib. Memo.* 2486.

Bruun, H. H. & Davies, P. O. A. L. 1975 *J. Sound Vib.* **40**, 535.

Durbin, P. A. 1979 Rapid Distortion Theory of Turbulent Flows. Ph.D. thesis. University of Cambridge.

Durbin, P. A. & Hunt, J. C. R. 1979 *5th Int. Conf. on Wind Engng, Univ. Colorado.*

Graham, J. M. R. 1976 *J. Fluid Mech.* **73**, 565.

Hawking, S. W. & Ellis, G. F. R. 1973 *Large Scale Structure of Space–Time*. Cambridge University Press.

Hunt, J. C. R. 1973 *J. Fluid Mech.* **61**, 625.

Hunt, J. C. R. 1974 *IUTAM-AHR Symp. on Flow Induced Vib., Karlsruhe, August* 1971. Springer.

Kawai, H., Junji, K. & Hatsuo, I. 1979 *5th Int. Conf. on Wind Engng, Univ. Colorado.*

Lamb, H. 1932 *Hydrodynamics*, 6th edn, Dover.

LEE, B. E. 1975 *J. Fluid Mech.* **69**, 263.

LIGHTHILL, M. J. 1956 *J. Fluid Mech.* **1**, 31.

LUMLEY, J. L. 1970 *Stochastic Tools in Turbulence.* Academic.

MARSHALL, S. 1965 Pressure fluctuation correlations near an axi-symmetric stagnation point. Ph.D. thesis, Colorado State University.

PARKINSON, G. V. & JANDALI, T. J. 1970 *J. Fluid Mech.* **40**, 577.

PROPPER, H. 1977 *Inst. Komst. Ing. Rhur Univ., Bochum, W. Germany, Tech. Rep.* 77–3.

TOWNSEND, A. A. 1976 *The Structure of Turbulent Shear Flow*, 2nd edn. Cambridge University Press.

TUNSTALL, M. J. 1974 *Proc. Symp. on Full Scale Fluid Dynamic Measurements, Leicester Univ.*